JBC RESEARCH ARTICLE

Protein arginine methyltransferase 5 is essential for oncogene product EWSR1-ATF1-mediated gene transcription in clear cell sarcoma

Received for publication, April 26, 2022, and in revised form, August 23, 2022 Published, Papers in Press, August 27, 2022,
https://doi.org/10.1016/j.jbc.2022.102434

Bingbing X. Li[1,2,*], **Larry L. David**[1,2], **Lara E. Davis**[2,3], **and Xiangshu Xiao**[1,2,*]

From the [1]*Department of Chemical Physiology and Biochemistry, Oregon Health & Science University, Portland, USA;* [2]*Knight Cancer Institute, Oregon Health & Science University, Portland, USA;* [3]*Division of Hematology and Medical Oncology, Department of Medicine, Oregon Health & Science University, Portland, USA*

Edited by Donita Brady

Transcription dysregulation is common in sarcomas driven by oncogenic transcription factors. Clear cell sarcoma of soft tissue (CCSST) is a rare sarcoma with poor prognosis presently with no therapy. It is characterized by a balanced t(12;22) (q13;q12) chromosomal translocation, resulting in a fusion of the Ewing's sarcoma gene *EWSR1* with activating transcription factor 1 (*ATF1*) to give an oncogene *EWSR1-ATF1*. Unlike normal ATF1, whose transcription activity is dependent on phosphorylation, EWSR1-ATF1 is constitutively active to drive ATF1-dependent gene transcription to cause tumorigenesis. No EWSR1-ATF1-targeted therapies have been identified due to the challenges in targeting intracellular transcription factors. Through proteomics screening to identify potential druggable targets for CCSST, we discovered protein arginine methyltransferase 5 (PRMT5) as a novel protein to interact with EWSR1-ATF1. PRMT5 is a type II protein arginine methyltransferase to symmetrically dimethylate arginine residues in substrate proteins to regulate a diverse range of activities including gene transcription, RNA splicing, and DNA repair. We found that PRMT5 enhances EWSR1-ATF1-mediated gene transcription to sustain CCSST cell proliferation. Genetic silencing of *PRMT5* in CCSST cells resulted in severely impaired cell proliferation and EWSR1-ATF1-driven transcription. Furthermore, we demonstrate that the clinical-stage PRMT5 inhibitor JNJ-64619178 potently and efficaciously inhibited CCSST cell growth *in vitro* and *in vivo*. These results provide new insights into PRMT5 as a transcription regulator and warrant JNJ-64619178 for further clinical development to treat CCSST patients.

Transcription dysregulation is common in sarcomas driven by oncogenic transcription factors (1). Clear cell sarcoma (CCS) of soft tissue (CCSST), first described in 1965 (2), is a rare but aggressive soft-tissue sarcoma that most often develops in the lower extremity close to tendons and aponeuroses of adolescents and young adults (2–4). The standard treatment for localized disease is to perform wide surgical resection or whole limb amputation. However, up to 85% of the patients develop the recurrence and eventual metastasis (2, 5). The 10-year overall survival rate is only ∼35%, and the 5-year survival rate is only ∼20% for metastatic disease (6–9). Since most of the patients are adolescents and young adults, the overall life years lost due to CCSST are more substantial. CCSST is notorious for its insensitivity to existing chemotherapies or radiation therapy. No therapies exist for CCSST.

The hallmark of CCSST is characterized by a balanced t(12;22) (q13;q12) chromosomal translocation, which results in a gene fusion between the Ewing's sarcoma gene *EWSR1* and activating transcription factor 1 (*ATF1*) to give an oncogene *EWSR1-ATF1* (10–12). EWSR1 is known as an RNA-binding protein (13). ATF1 is a member of the cAMP-responsive element (CRE)–binding protein (CREB) family transcription factors (14, 15). The gene fusion retains the C-terminal basic leucine-zipper (bZIP) DNA-binding domain of ATF1. The CREB family of transcription factors requires phosphorylation at Ser133 of CREB1 or Ser63 of ATF1 by protein Ser/Thr kinases including cAMP-regulated protein kinase A (PKA) in order to be transcriptionally active (16). However, in the case of EWSR1-ATF1 fusion, the serine-tyrosine-glycine-glutamine (SYGQ)–rich domain present in the N-terminal portion of EWSR1 is a strong transcription activation domain (17). Therefore, EWSR1-ATF1 is constitutively active in driving CREB1/ATF1-depenent gene transcription through its bZIP domain independent of phosphorylation (18).

Genetic mouse modeling studies have established that expression of EWSR1-ATF1 is sufficient to drive the development of CCSST in mice, resembling human pathologies (19–21). Besides the initial discovery of type 1 *EWSR1-ATF1* fusion in CCSST patients, 6 other types of *EWSR1-ATF1* fusion and *EWSR1-CREB1* have also been reported in CCSST patients (22). Furthermore, these gene fusions have been observed in other CCS-like disease pathologies in other parts of the body including the gastrointestinal tract and other abdominal surfaces (5). Together, the identification of *EWSR1-ATF1* and *EWSR1-CREB1* fusion underscores the critical role of constitutive CREB1/ATF1-mediated gene transcription in

* For correspondence: Bingbing X. Li, lib@ohsu.edu; Xiangshu Xiao, xiaoxi@ohsu.edu.

the development of CCSST and other CCS-like cancers that lack effective therapies. However, it is unclear how EWSR1-ATF1 can activate CREB1/ATF1-dependent gene transcription without phosphorylation. Lack of this mechanistic understanding inhibits our capability to identify novel therapeutics for these sarcomas. In this paper, we describe the identification of protein arginine methyltransferase 5 (PRMT5) as a new EWSR1-ATF1 binding co-activator to stimulate its transcription activity. We further employed genetic and chemical means to inhibit PRMT5 to demonstrate that PRMT5 is a novel druggable vulnerability in EWSR1-ATF1-driven CCSST.

Results

EWSR1-ATF1 is constitutively active in driving CREB1/ATF1-mediated gene transcription

The most common fusion between EWSR1 and ATF1 generates EWSR1(2–325)-ATF1(66–271) fusion containing N-terminal portion of EWSR1 and C-terminal portion of ATF1 with its intact bZIP DNA-binding domain (23). Genetic studies have provided compelling evidence that the growth and survival of CCSST cells are critically dependent on the continuous expression of EWSR1-ATF1 and its transcription activity (19, 24). As a fusion protein between an RNA-binding protein EWSR1 and a transcription factor ATF1, the major portion of EWSR1-ATF1 fusion protein is predicted to be unstructured. Indeed, when the fusion protein sequence was analyzed by PONDR (Predictor of Natural Disordered Regions) algorithm (25), the majority of the EWSR1 region is found to be unstructured (Fig. 1*A*). As expected, the bZIP domain in the C-terminal portion of ATF1 is ordered. Consistent with this prediction, the artificial intelligence (AI) algorithm AlphaFold (26) also predicts that EWSR1 portion is unstructured, while a good fraction of ATF1 including the bZIP domain is structured (Fig. 1*B*). Even within the structured region of ATF1, no obvious small-molecule-binding sites can be readily identified (Fig. S1*A*). As a consequence, direct targeting of EWSR1-ATF1 by small molecules is challenging and no direct small-molecule inhibitors of EWSR1-ATF1 have been developed.

Despite EWSR1-ATF1 being largely unstructured, it has been reported that it functions as a constitutively active transcription factor (18). To confirm this, we created the in-frame Flag-tagged fusion between EWSR1(2–325) and ATF1(66–271) (Fig. S1*B*). When EWSR1-ATF1 was expressed along with our previously described CREB1/ATF1 transcription reporter plasmid (CRE-RLuc) in HEK 293T cells (27), we found that the exogenously expressed EWSR1-ATF1 is transcriptionally active in driving CREB1/ATF1-depedent gene transcription (Fig. 1*C*). Furthermore, this transcription activity is independent of phosphorylation as adding PKA activator forskolin (Fsk) did not further enhance its transcription activity (Fig. 1*D*). These results support that EWSR1-ATF1 is constitutively active in driving CREB1/ATF1-dependent gene transcription.

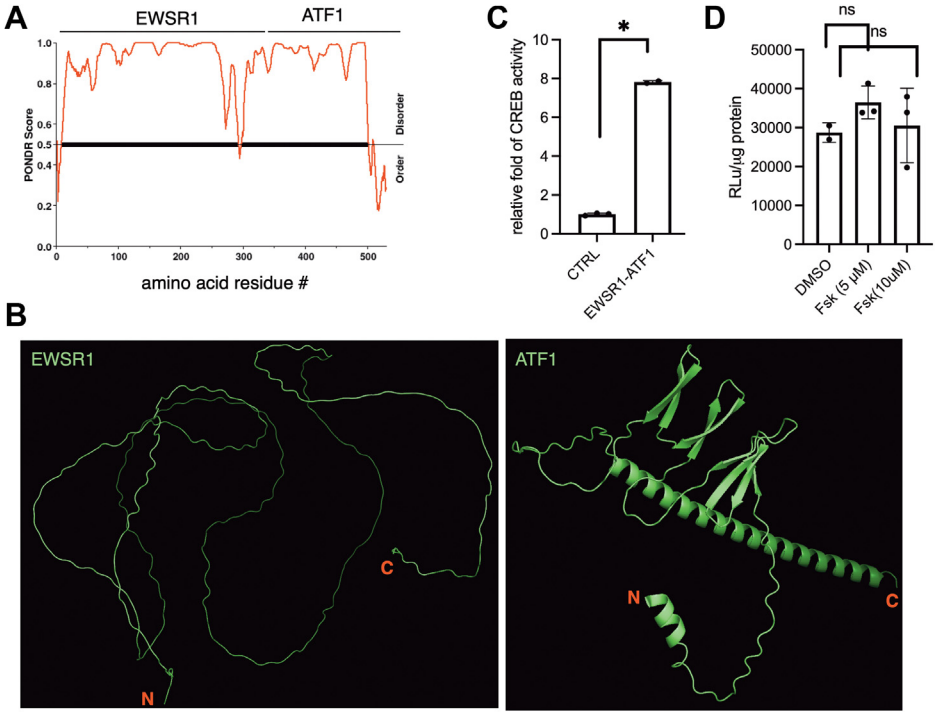

Figure 1. EWSR1-ATF1 is unstructured and constitutively active in driving CREB1/ATF1-dependent gene transcription. *A*, the major portion of EWSR1-ATF1 is predicted to be unstructured. The PONDR score was calculated using online PONDR server at http://www.pondr.com. *B*, cartoon presentation of AlphaFold predicted structures of EWSR1(2–325) (left) and ATF1(66–271) (right). The N- and C-termini are labeled. *C*, EWSR1-ATF1 is constitutively active. HEK 293T cells were transfected with an empty vector or EWSR1-ATF1 along with CREB1 transcription reporter plasmid CRE-RLuc. Then, the renilla luciferase activity was measured and normalized to the protein content. *D*, EWSR1-ATF1's transcription activity is independent of phosphorylation. HEK 293T cells were transfected with EWSR1-ATF1 along with CREB1 transcription reporter plasmid CRE-RLuc. The cells were treated with different concentration of forskolin (Fsk) for 5 h before the renilla luciferase activity was measured, which was further normalized to the protein content. * $p < 0.05$.

EWSR1-ATF1 interacts with PRMT5

Since EWSR1-ATF1 has been established as the genetic driver for CCSST development and maintenance, targeting this driver represents a potentially promising approach to develop effective therapeutics. However, the lack of a well-folded structural pocket for small-molecule binding in EWSR1-ATF1 creates challenges in developing direct small-molecule inhibitors to inhibit its transcription activity as potential therapeutics. To circumvent this intrinsic challenge, we sought to identify critical proteins that would interact with EWSR1-ATF1 to support its constitutive transcription activity and hypothesized that these proteins might serve as potential drug targets for CCSST. Therefore, we expressed Flag-tagged EWSR1-ATF1 in HEK 293T cells. To identify the proteins that would interact with EWSR1-ATF1, the expressed EWSR1-ATF1 was subjected to immunoprecipitation by anti-Flag (M2) followed by mass spectrometry (IP-MS) analysis (Fig. 2*A*). An IgG control pulldown was also included. This analysis identified 157 proteins that presented higher abundance in the anti-Flag sample (Table S1). Gene ontology (GO) analysis of these 157 proteins in the biological processes using g:Profiler (28) revealed that many processes involving RNA molecules are enriched (Table S2). The top 15 biological processes enriched are shown in Fig. 2*B*, which include both RNA catabolic and metabolic processes. Among these processes, the mRNA metabolic process contains protein arginine methyltransferase 5 (PRMT5) that has recently become a druggable target (29). Various PRMT5 inhibitors have been developed, and at least 5 of them are in phase 1/2 clinical trials for different malignancies (30). Additionally, PRMT5 is one of only 6 proteins (PPM1B, KIF11, PRMT5, ACTR3, HBB, and PTGES3) that interact with EWSR1-ATF1 specifically and have 3 or more unique peptide identifications (Fig. 2*C*, S2 and Table S1). Furthermore, while PRMT5 has not previously been shown to interact with EWSR1-ATF1, it was reported that PRMT5 could function as a transcription co-activator for CREB1 in hepatocytes to enhance CREB1-mediated gene transcription (31). For these reasons, we focused our

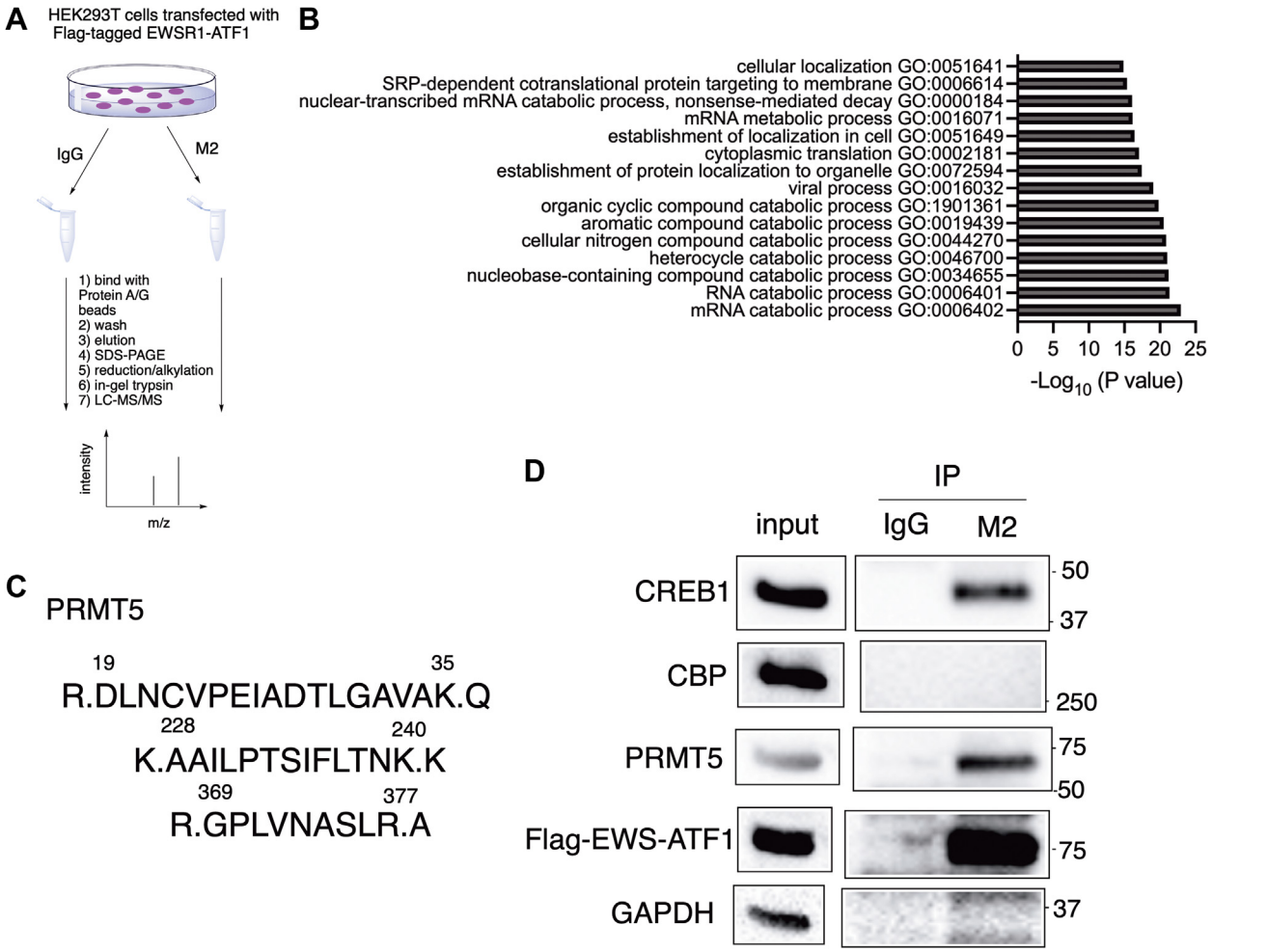

Figure 2. EWSR1-ATF1 interacts with PRMT5. *A*, a schematic diagram of IP-MS/MS to identify proteins that interact with EWSR1-ATF1. *B*, top 15 enriched biological processes by GO analysis of the 157 proteins interacting with EWSR1-ATF1 using g:Profiler. The enriched biological processes were rank ordered by adjusted *p* values. See Table S2 for the full list. *C*, identification of PRMT5 to interact with EWSR1-ATF1. HEK 293T cells were transfected with Flag-tagged EWSR1-ATF1. Then, the lysates were prepared for co-immunoprecipitation (co-IP) using either IgG or anti-Flag (M2). The eluted proteins were analyzed by LC-MS/MS. The identified peptides corresponding to PRMT5 are shown (from M2 IP). No peptides corresponding to PRMT5 were identified in the IgG immune complex. *D*, validation of the interaction between EWSR1-ATF1 and PRMT5. Flag-tagged EWSR1-ATF1 was expressed in HEK 293T cells and the lysates were processed in the same way as in (*A*). The bound proteins were analyzed by Western blot using indicated antibodies.

investigation on PRMT5 as a putative critical target for EWSR1-ATF1-driven CCSST.

PRMT5 is a type II protein arginine methyltransferase leading to symmetric arginine dimethylation of both histone and non-histone proteins to regulate a diverse range of activities including gene transcription, RNA splicing, and DNA repair (32). To confirm the proteomics findings, we expressed Flag-tagged EWSR1-ATF1 in HEK 293T cells and immunoprecipitated the cell lysates using anti-Flag antibody (M2). Then, the bound proteins were analyzed by Western blot. Indeed, strong PRMT5 signal was detected in the M2 immunoprecipitate, but not in the control IgG immunoprecipitate (Fig. 2*D*). CREB1 can form a heterodimer with the C-terminal domain of ATF1 through its bZIP domain that is retained in EWSR1-ATF1. Indeed, CREB1 was detected in the M2 immune complex (Fig. 2*D*). Conflicting reports exist to show that EWSR1-ATF1 constitutively interacts with CREB-binding protein (CBP) to support its constitutive transcription activity (33, 34). In our co-IP analysis, the constitutive interaction between EWSR1-ATF1 and CBP was not detected. As a control, GAPDH was not detected in either of the immune complexes (Fig. 2*B*). Together, these results demonstrate that EWSR1-ATF1 interacts with PRMT5 in the cells to possibly function as a transcription co-activator to support EWSR1-ATF1-mediated gene transcription.

PRMT5 is critical for EWSR1-ATF1-mediated gene transcription

The results presented above suggest that PRMT5 might be a potential transcription co-activator for EWSR1-ATF1. To test if PRMT5 is bound to the gene promoter region of EWSR1-ATF1 target gene *c-Fos* (24) in CCSST cells, chromatin immunoprecipitation (ChIP) was performed in CCSST cell line DTC-1. After the cells were cross-linked with formaldehyde, they were subjected to ChIP analysis using IgG, anti-CREB1, or anti-PRMT5. CREB1 forms a heterodimer with EWSR1-ATF1 (Fig. 2*D*) and served as a positive control for the ChIP assay. Indeed, the CRE site in the *c-Fos* promoter region is occupied by CREB1 (Fig. 3*A*). Importantly, this site is also occupied by PRMT5 (Fig. 3*A*), suggesting that PRMT5 may enhance EWSR1-ATF1's transcription activity by binding to the promoter region of its target genes.

To investigate if PRMT5 is required for sustained transcription of *c-Fos* in CCSST cells, its expression was silenced in SU-CCS-1 cells using two different shRNA constructs. Both of these constructs efficiently knocked down the expression of PRMT5 (Fig. 3*B*). When the expression of PRMT5 was reduced, the expression of EWSR1-ATF1's target gene *c-Fos* was also significantly reduced, as assessed by quantitative reverse transcription-polymerase chain reaction (qRT-PCR) analysis (Fig. 3*C*), suggesting that PRMT5 is critical for enhancing EWSR1-ATF1's transcription activity. Similar

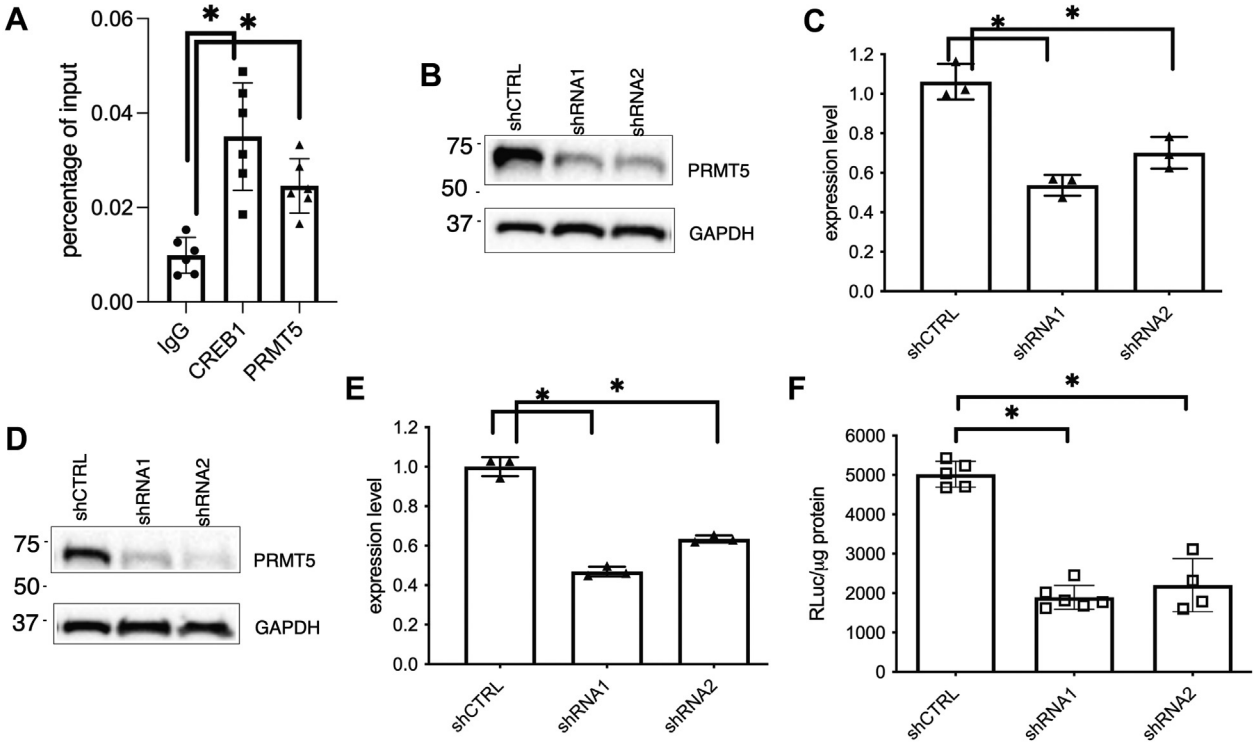

Figure 3. PRMT5 is critical for EWSR1-ATF1-mediated gene transcription. *A*, PRMT5 is bound to the *c-Fos* promoter in DTC-1 cells. DTC-1 cells were subjected to ChIP assay protocol as described in the Experimental procedures. The enriched DNA by individual antibodies was analyzed by qPCR analysis. *B*, the expression of *PRMT5* was silenced using two different shRNA constructs in SU-CCS-1 cells. *C*, the expression of *c-Fos* was reduced with sh*PRMT5*. SU-CCS-1 cells were transduced with indicated lentiviruses expressing different shRNA constructs. The total RNA was collected for qRT-PCR analysis. *D*, silencing *PRMT5* expression in DTC-1 cells using shRNA. DTC-1 cells were transduced with lentiviruses expressing indicated shRNA constructs. The lysates were prepared for Western blot analysis using indicated antibodies. *E*, silencing *PRMT5* expression in DTC-1 cells decreased mRNA level of *c-Fos*. The cells transduced with shRNA lentiviruses were processed for qRT-PCR analysis for quantification of *c-Fos* transcript. *F*, EWSR1-ATF1-driven CRE-RLuc expression is reduced by sh*PRMT5*. DTC-1 cells were transduced with lentiviruses expressing CRE-RLuc along with lentiviruses expressing indicated shRNA. Then, the renilla luciferase activity was quantified and normalized to protein concentration under each condition. * $p < 0.05$.

knocking down results were also obtained in another CCSST cell line DTC-1 (Fig. 3, *D* and *E*). We further evaluated PRMT5's role in supporting EWSR1-ATF1-mediated gene transcription using a CREB1/ATF1 transcription reporter assay in DTC-1 cells. The cells were transduced with a lentivirus containing renilla luciferase reporter gene under the control of three tandem copies of CRE that could bind EWSR1-ATF1 (27). Upon *PRMT5* knockdown by two different shRNAs, the CREB1/ATF1 transcription reporter activity was significantly reduced (Fig. 3*F*). These evaluations of the transcription reporter and endogenous gene expression in CCSST cells showed that PRMT5 is critical for the constitutive EWSR1-ATF1-driven transcription.

PRMT5 inhibition leads to CCSST cell growth inhibition

Because EWSR1-ATF1-driven transcription is critical for sustained CCSST cell proliferation, we investigated if silencing the expression of *PRMT5* would impact CCSST cellular proliferation. To this end, the expression of *PRMT5* was silenced in both SU-CCS-1 and DTC-1 cells using two independent shRNA constructs. Upon *PRMT5* knockdown (Fig. 3, *B* and *D*), the proliferation of both SU-CCS-1 and DTC-1 cells was significantly impaired (Fig. 4*A*), suggesting that PRMT5 is critical for the proliferation of CCSST cells.

Given the potentially important role of PRMT5 in CCSST cells and druggability of PRMT5 (29), we investigated the potential efficacy of PRMT5 inhibitors in inhibiting CCSST cell growth. We selected 3 highly potent and selective PRMT5 inhibitors representing two different modes of inhibition of PRMT5 to assess their efficacy in CCSST models. **GSK591** and **GSK3326595** bind at the protein substrate-binding pocket (35, 36), while **JNJ-64619178** binds simultaneously to the *S*-adenosyl methionine (SAM)- and protein substrate-binding pockets (Figs. 4*B* and S3) (37). The inhibitors were tested in 3 different CCSST cell lines: SU-CCS-1, DTC-1, and CCS292. The cells were incubated with different PRMT5 inhibitors for either 3 days or 6 days. Then, viable cells were quantified using the MTT reagent and the GI_{50} values were calculated, which are the concentrations needed to inhibit the cell growth by 50% (38). As shown in Fig. 4*C* and Fig. S4, *A*–*C*, different PRMT5 inhibitors showed differential sensitivity profiles in the panel of CCSST cell lines. **GSK591** and **GSK3326595** were only weakly active in DTC-1 and SU-CCS-1 cells with GI_{50}s in the high μM concentration range although its activity in CCS292 cells was much more potent. On the other hand, **JNJ-64619178** displayed more potent activities in both DTC-1 and SU-CCS-1 cells with GI_{50} = 377 and 347 nM, respectively, during a 3-day incubation period. Thus, **JNJ-64619178** was further evaluated in a 6-day treatment protocol. Upon this extended exposure, **JNJ-64619178** showed dramatically improved activity with GI_{50} = 29.3, 445.8, and 3.8 nM in DTC-1, SU-CCS-1, and CCS292 cells, respectively (Fig. 4*C* and S4*D*). While all the three inhibitors are highly potent in inhibiting the methyltransferase activity of PRMT5 (35–37), the differential sensitivity profile among the different PRMT5 inhibitors in CCSST cells suggests that the different binding modes of these inhibitors can uniquely modulate EWSR1-ATF1-mediated gene transcription. During the preparation of this manuscript, additional PRMT5 inhibitors became available. Therefore, we evaluated another clinical-stage SAM-competitive PRMT5 inhibitor **PF-0693999** (39) and 3 other tool PRMT5 inhibitors (**CMP5** (40), **EPZ015666** (35), and **BRD0639** (41)) in CCSST cells. **CMP5** is predicted to be SAM-competitive. Similar to **GSK591** and **GSK3326595**, **EPZ015666** binds to the substrate-binding pocket. **BRD0639** is unique in that it covalently binds to a site distal to the catalytic site. As shown in Fig. S5, these additional inhibitors presented varied potencies in the CCSST cells. But they are all less potent than **JNJ-64619178**, further supporting that differential binding modes can contribute to the differential sensitivity irrespective of their potencies in biochemical PRMT5 inhibition.

JNJ-64619178's potent growth inhibitory activity in CCSST cells prompted us to further test its capability to inhibit EWSR1-ATF1-mediated gene transcription. In the CREB1/ATF1 transcription reporter assay in DTC-1 cells, **JNJ-64619178** displayed an IC_{50} of 422 nM (Fig. 4*D*). Consistent with the low potency of GSK compounds in inhibiting CCSST cell growth, neither of these two substrate-competitive inhibitors significantly inhibited EWSR1-ATF1's transcription activity (Fig. 4*E*), further emphasizing the unique mechanism of action of **JNJ-64619178** in CCSST cells. Altogether, these results support a critical role of PRMT5 in enhancing EWSR1-ATF1's transcription activity for sustained cell growth in CCSST cells and suggest that PRMT5 is a potential novel druggable vulnerability in CCSST cells.

JNJ-64619178 inhibits EWSR1-ATF1-mediated gene transcription and CCSST tumor growth in vivo

The results presented above strongly suggest that **JNJ-64619178** may represent a novel therapeutic agent for the deadly CCSST. We first examined if **JNJ-64619178** could downregulate the expression of endogenous EWSR1-ATF1's target gene in SU-CCS-1 cells. When the cells were treated with **JNJ-64619178**, we observed that **JNJ-64619178** dose-dependently inhibited transcription of *c-Fos* (Fig. 5*A*). **JNJ-64619178** treatment in DTC-1 cells caused a similar decrease in the mRNA level of *c-Fos* (Fig. 5*B*). Decreased transcription of *c-Fos* by **JNJ-64619178** in SU-CCS-1 and DTC-1 cells led to a decrease of c-Fos protein abundance (Fig. 5*C*). Taken together, these results showed that **JNJ-64619178** potently inhibited EWSR1-ATF1-mediated gene transcription in CCSST cells, leading to impaired CCSST cell growth.

Encouraged by the promising activities seen with **JNJ-64619178** in inhibiting EWSR1-ATF1-mediated gene transcription and inhibiting CCSST cell growth *in vitro*, we further investigated its anticancer efficacy in an *in vivo* xenograft model. SU-CCS-1 cells were injected subcutaneously into immunodeficient mice (female:male = 1:1). When the tumor was well established and reached a size of ~100 mm^3, the mice were randomized to receive either vehicle or **JNJ-64619178** at 10 mg/kg by intraperitoneal

injection. The daily treatment lasted for 5 weeks, and the tumor volumes were measured every 2 to 3 days. As shown in Fig. 5*D*, this tumor grew very aggressively when the mice were treated with a vehicle solution. On the other hand, when the mice were treated with **JNJ-64619178**, the tumor growth was essentially completely inhibited. While the tumors in the vehicle group grew 5- to 25-fold, the tumors in the treated group were either only slowly growing or regressed in this aggressive xenograft (Fig. 5*E*). During the entire course of treatment period, no change of body weight (Fig. 5*F*) or other toxicity was observed, consistent with its safety profile observed in other models (37). These results support that the PRMT5 inhibitor **JNJ-64619178** represents a potential treatment option for CCSST.

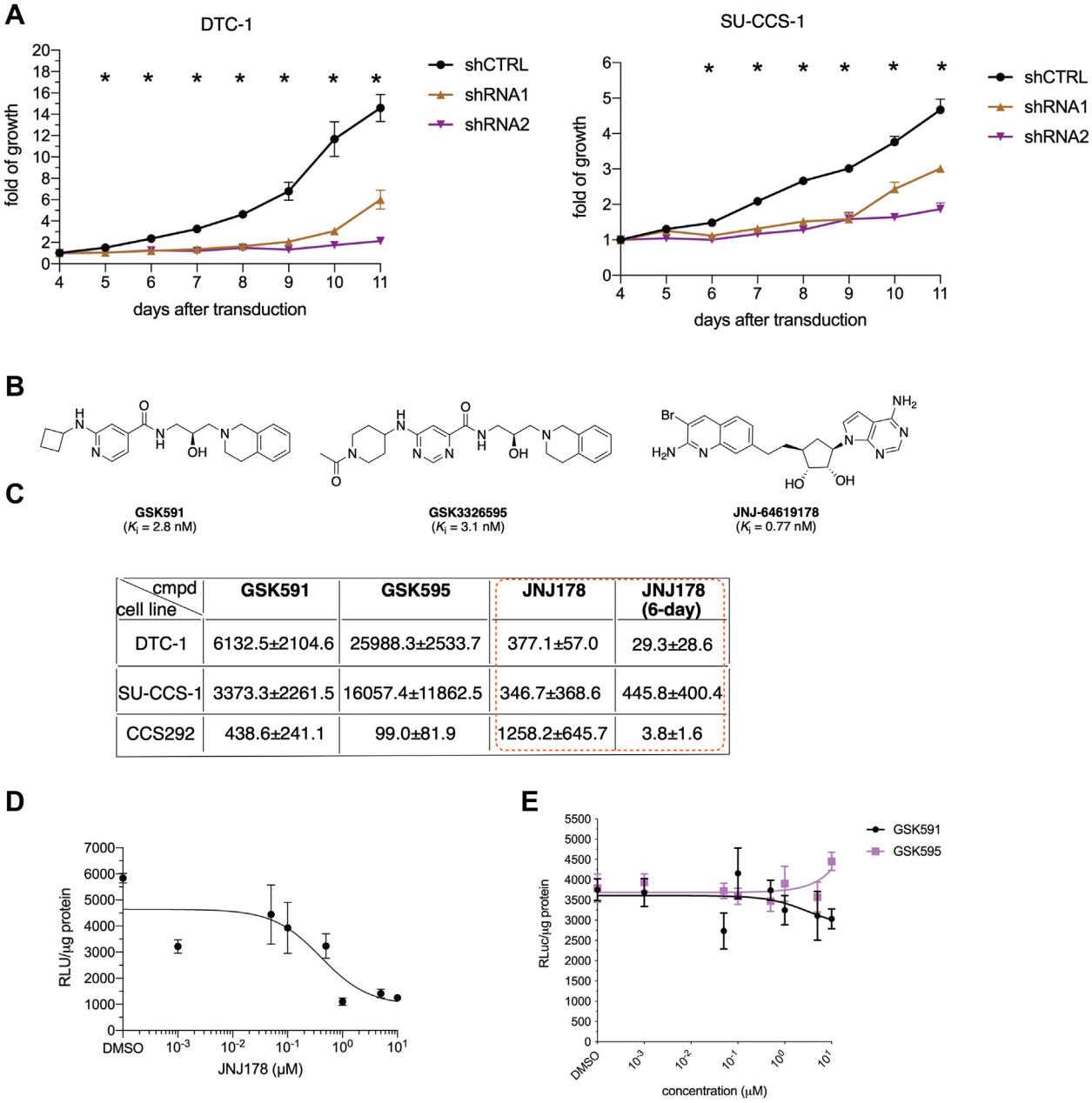

cmpd / cell line	GSK591	GSK595	JNJ178	JNJ178 (6-day)
DTC-1	6132.5±2104.6	25988.3±2533.7	377.1±57.0	29.3±28.6
SU-CCS-1	3373.3±2261.5	16057.4±11862.5	346.7±368.6	445.8±400.4
CCS292	438.6±241.1	99.0±81.9	1258.2±645.7	3.8±1.6

Figure 4. Inhibition of PRMT5 leads to impaired CCSST cell growth. *A*, silencing *PRMT5* expression resulted in reduced cellular proliferation in DTC-1 (left) and SU-CCS-1 (right) cells. The cells were transduced with indicated shRNA constructs. After 3 days, the cell growth was analyzed by the MTT reagent over a period of 8 days. *B*, chemical structures of PRMT5 inhibitors to be used in this paper. Their apparent inhibition constants K_i are shown and from published references. *C*, summary of the GI_{50}s (nM) of 3 different PRMT5 inhibitors in 3 different CCSST cell lines. The cells were treated with different concentrations of the indicated compounds for either 3 days or 6 days (as indicated). Then, the remaining viable cells were quantified by the MTT reagent. The values represent the mean ± SD of at least 2 independent experiments performed in triplicates. See Fig. S4 for their respective dose-response curves. *D*, **JNJ-64619178** inhibited EWSR1-ATF1-mediated gene transcription in DTC-1 cells. DCT-1 cells with CRE-RLuc reporter integration were treated with different concentrations of **JNJ-64619178** for 24 h. Then, the remaining renilla luciferase activity was measured and normalized to protein content in each well. *E*, **GSK591** and **GSK3326595** did not inhibit EWSR1-ATF1-mediated gene transcription in DTC-1. DTC-1 cells with CRE-RLuc were treated with different concentrations of GSK compounds for 24 h. Then, the remaining renilla luciferase activity was measured and normalized for protein content in each well. * $p < 0.05$.

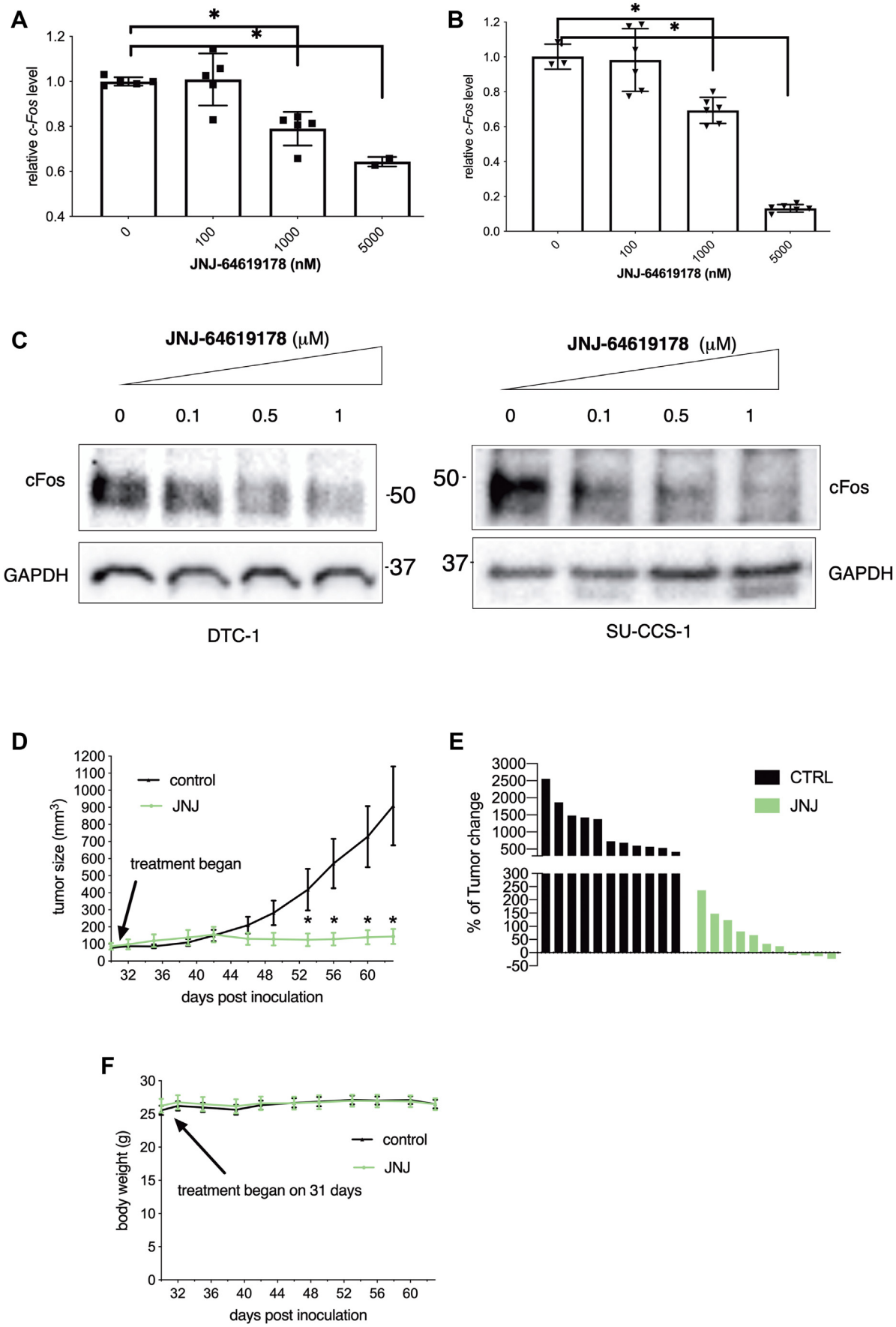
A
relative c-Fos level
JNJ-64619178 (nM)
B
relative c-Fos level
JNJ-64619178 (nM)
C
JNJ-64619178 (μM)
0 0.1 0.5 1
cFos
GAPDH
DTC-1
SU-CCS-1
D
tumor size (mm3)
control
JNJ
treatment began
days post inoculation
E
% of Tumor change
CTRL
JNJ
F
body weight (g)
control
JNJ
treatment began on 31 days
days post inoculation

Discussion

CCSST remains a deadly disease with no therapy. While the driver oncogene *EWSR1-ATF1* has been clearly identified, the predicted flexible structural nature of EWSR1-ATF1 has made it recalcitrant for direct targeting using cell-permeable small molecules with appropriate drug-like properties. Due to its rare nature, it has been largely neglected to develop novel therapies. No standard systemic therapies exist. No targeted therapies have been identified as effective treatments for CCSST. No validated druggable targets have been identified for EWSR1-ATF1-driven CCSST. Previous studies have suggested that receptor tyrosine kinase c-Met might be a potential target for CCSST (42). However, c-Met has not been shown to modulate EWSR1-ATF1-driven gene transcription, the driver of CCSST (42). Furthermore, clinical studies using c-Met inhibitor crizotinib failed to produce meaningful benefits to CCS patients (43). Here, we identified PRMT5 as a critical protein to interact with EWSR1-ATF1 to enhance EWSR1-ATF1-mediated gene transcription and supporting CCSST cell growth, lending support that PRMT5 is a novel druggable target for EWSR1-ATF1-driven CCSST. Genetic silencing of *PRMT5* robustly inhibited CCSST tumor cell growth and EWSR1-ATF1-driven gene transcription. By targeting PRMT5 using different inhibitors, we further identified **JNJ-64619178** as a potential novel treatment option for CCSST. Interestingly, we found that the PRMT5 inhibitors based on **GSK591** are not effective in inhibiting EWSR1-ATF1-mediated gene transcription, suggesting that **JNJ-64619178** can uniquely impact the EWSR1-ATF1-PRMT5 complex at the gene promoter region to inhibit its transcription activity. Our results provide new insights into the role of PRMT5 as a transcription regulator. The different PRMT5 inhibitors with different modes of inhibition will be useful for our further understanding of PRMT5's functions. Since the clinical development of **JNJ-64619178** for other oncology indications is ongoing (clinical trial # NCT03573310), the results presented here provide compelling evidence to further clinically evaluate this PRMT5 inhibitor for EWSR1-ATF1-driven and deadly CCSST and other CCS-like malignancies.

Experimental procedures

Plasmids and antibodies

The CREB1/ATF1 reporter construct CRE-RLuc was reported previously by us (27). Flag-tagged EWSR1-ATF1 expression vector was generated by In-Fusion Snap Assembly Master Mix (Takara) to fuse EWSR1 (2–325) in-frame with ATF1 (66–271) into pEGFP-N_3 (Clontech). The EWSR1 (2–325) and ATF1 (66–271) fragments were PCR amplified from their respective open reading frames obtained from DNASU plasmid repository (Arizona State University). Lentiviral construct CRE-RLuc was prepared by gene synthesis followed by subcloning into pLJM1 vector (Addgene). All lentiviral shPRMT5 plasmids were purchased from Millipore Sigma. The lentiviral packaging vectors (pMD2.G and pMDLg/pRRE) were from Addgene. The following antibodies were used: anti-Flag (M2) (Sigma), anti-PRMT5 (Santa Cruz Biotechnology and Millipore), anti-GAPDH (Santa Cruz Biotechnology), anti-CREB1 (Cell Signaling Technology), anti-c-Fos (Cell Signaling Technology), anti-CBP (Santa Cruz Biotechnology).

Cell lines

HEK293T and SU-CCS-1 were obtained from ATCC. DTC-1 was a kind gift from Prof. Torsten Nielsen (University of British Columbia). CCS-292 was a generous gift from Prof. Charles Keller (Children's Cancer Therapy Development Institute). The cells were maintained in Dulbecco's Modified Eagle Medium (DMEM, Life Technologies) supplemented with 10% fetal bovine serum (Hyclone) and nonessential amino acids (Life Technologies). *Mycoplasma* contamination was tested regularly with MycoDect Mycoplasma Detection Kit (ALSTEM). All the cell lines have been authenticated using short tandem repeat profiling.

Chemicals

GSK591, **GSK3326595**, **BRD0639**, and **EPZ015666** were obtained MedChemExpress LLC. **PF-06939999** was purchased from Chemietek. **CMP5** was obtained from Sigma. **JNJ-64619178** was obtained from ChiralStar. For *in vitro* assays, the drugs were dissolved in dimethyl sulfoxide (DMSO) as stock solutions. For *in vivo* treatment, **JNJ-64619178** was dissolved in 1% *N*-methyl-2-pyrrolidone, 5% DMSO, and 5% Tween-80 in ddI H_2O.

Lentivirus preparation and transduction

The lentiviruses were prepared and used in a similar way as previously described (44). Briefly, lentiviruses expressing CRE-RLuc or indicated shRNA were prepared from HEK 293T cells by co-transfecting lentiviral expression plasmids along with packaging vectors using the calcium-phosphate method (TakaRa). DTC-1 cells were transduced with lentiviruses expressing CRE-RLuc. After puromycin selection, the cells were used directly for reporter assays.

Figure 5. JNJ-64619178 inhibited EWSR1-ATF1-mediated gene transcription and displayed anti-CCSST activity *in vitro* and *in vivo*. *A*, **JNJ-64619178** inhibited *c-Fos* transcription in SU-CCS-1 cells. The cells were treated with different concentrations of **JNJ-64619178** for 24 h. Then, the total RNA was isolated and converted into cDNA. The relative *c-Fos* transcript level was quantified by qRT-PCR using *18S* as a reference gene. *B*, **JNJ-64619178** decreased *c-Fos* mRNA level in DTC-1 cells. The cells were treated with **JNJ-64619178** for 12 h. Then, the total RNA was isolated and the relative *c-Fos* mRNA level was analyzed by qRT-PCR using *18S* as the reference gene. *C*, **JNJ-64619178** decreased c-Fos protein level in SU-CCS-1 and DTC-1 cells. The cells were treated with different concentrations of **JNJ-64619178** for 24 h. Then, the whole-cell lysates were prepared for Western blot analyses using indicated antibodies. *D*, **JNJ-64619178** efficaciously inhibited SU-CCS-1 tumor growth *in vivo*. SU-CCS-1 cells were implanted subcutaneously in athymic nude mice (male:female = 1:1). When the tumor sizes reached an average of ~100 mm^3, the mice were randomized to be treated with either vehicle or **JNJ-64619178** at 10 mg/kg (QDX5 weeks). The tumor volume was measured every 2 to 3 days. *E*, waterfall plot of the tumor volume change at the end of treatment in (*D*). *F*, **JNJ-64619178** treatment in mice did not change the body weights. The body weights of the treated mice in (*D*) were measured every 2 to 3 days * $p < 0.05$.

shRNA silencing

SU-CCS-1 and DTC-1 cells were transduced with indicated lentiviruses expressing shCTRL or shPRMT5 for 24 h, when fresh media were added for another 48 h. Then, the cells were used for the following experiments: cell growth assay by MTT, whole cell lysates for Western blot, and total RNA for qRT-PCR assays.

qRT-PCR

The cells were treated with indicated drugs. Then, the cells were collected using the cell lysis buffer provided in Nucleo-Spin RNA (Takara). The total RNA was isolated following the manufacturer's instructions. First strand cDNA was synthesized with PrimeScript 1st strand cDNA synthesis kit (Takara). Quantitative PCR reactions were performed using TB Green Advantage qPCR Premix (Takara) in QuantStudio 7300 (Life Technologies). The $2^{-\Delta\Delta Ct}$ method was used to determine the relative expression level. The following primers were used: *18S*: 5′- GGATGTAAAGGATGGAAAATACA-3′ (forward), 5′- TCCAGGTCTTCACGGAGCTTGTT-3′ (reverse); *c-Fos*: 5′-GGAGGAGGGAGCTGACTGAT-3′ (forward), 5′- GAGC TGCCAGGATGAACTCT-3′ (reverse).

Transcription reporter assay

For transient transfections, HEK 293T cells were transfected with CRE-RLuc along with Flag-EWSR1-ATF1 using Lipofectamine2000 (Life Technologies) following the manufacturer's instructions. Twenty-four hours post transfection, the cells were lysed using Renilla luciferase lysis buffer, and the renilla luciferase activity was measured using Renilla luciferase assay system (Promega) in FB12 single tube luminometer (Berthold). For reporter assay in DTC-1 cells with stable CRE-RLuc integration, the cells were treated with indicated drugs at different concentrations for 24 h. The remaining renilla luciferase activity was measured as above. All the luciferase activity was normalized to protein concentration in each well and expressed as RLuc/μg protein.

IP-MS and IP-western blot

HEK 293T cells were transfected with Flag-EWSR1-ATF1 using Lipofectamine2000 (Life Technologies). Twenty-four hours post transfection, the cells were harvested and washed twice with cold PBS. Then, the cell pellets were lysed in lysis buffer A (50 mM Tris, 5 mM EDTA, 150 mM NaCl, 1 mM DTT, 0.5% Nonidet P-40, pH 8.0) supplemented with protease inhibitor cocktail (Roche) and 1 mM PMSF. The cell lysates were precleared with 1 μg of mouse IgG (Rockland Immunochemicals) and protein A/G agarose beads (Pierce) for 1 h at 4 °C with tumbling. The precleared lysates were then incubated with either mouse IgG or M2 for overnight at 4 °C. Then, protein A/G agarose bead slurry was added to precipitate the immune complexes for 1 h at 4 °C. The bound immune complex was washed with lysis buffer A (3×) and the bound proteins were eluted from the beads using 1%SDS in PBS. The eluted proteins were analyzed by protein LC-MS/MS or Western blot.

Protein LC-MS/MS

Immunoprecipitated proteins from above were dried by vacuum centrifugation. They were then redissolved in 20 μl of 1× SDS-PAGE sample buffer, applied to wells of a NuPAGE 10% Bis-Tris SDS-PAGE gel (NP0301BOX), electrophoresed for 6 min at 200 V, and stained for 30 min with Imperial Blue protein stain (catalog no. 24615; Thermo Scientific). The gel was then rinsed in water, and the entire top 1 cm of each lane containing proteins was excised, cut into 1-mm pieces, reduced/alkylated, and digested with trypsin for 1 hour at 50 °C in the presence of 0.01% ProteaseMax detergent using the method recommended from the manufacturer (Promega). Recovered peptides were then filtered using 0.22-μm Millipore Ultrafree-CL centrifugal filters. The filtrate was dried by vacuum centrifugation and then redissolved in 20 μl of 5% formic acid in preparation for mass spectrometric analysis.

Each digest was then chromatographically separated using a Dionex RSLC UHPLC system and delivered to a Q-Exactive HF mass spectrometer (Thermo Scientific) using electrospray ionization with a Nano Flex Ion Spray Source fitted with a 20-μm stainless-steel nano-bore emitter spray tip and 1.0-kV source voltage. Xcalibur version 4.0 was used to control the system. Samples were applied at 10 μl/min to a Symmetry C18 trap cartridge (Waters) for 5 min and then switched onto a 75 μm x 250 mm NanoAcquity BEH 130 C18 column with 1.7 μm particles (Waters) using mobile phases water (A) and acetonitrile (B) containing 0.1% formic acid, 7.5 to 30% acetonitrile gradient over 60 min, and 300 nl/min flow rate. Survey mass spectra were acquired over m/z 375 – 1400 at 120,000 resolution (m/z 200), and data-dependent acquisition selected the top 10 most abundant precursor ions for tandem mass spectrometry by HCD fragmentation using an isolation width of 1.2 m/z, normalized collision energy of 30, and a resolution of 30,000. Dynamic exclusion was set to auto, charge state for MS/MS +2 to +7, maximum ion time 100 ms, and minimum AGC target of 3×10^6 in MS1 mode and 5×10^3 in MS2 mode.

Comet (v. 2016.01, rev. 2) (45) was used to search 29,088 MS2 Spectra against a UniProt FASTA protein database (downloaded from www.uniprot.org November 2018) containing 21,080 canonical *Homo sapiens* sequences. An additional 179 common contaminant sequences were added, and sequence-reversed decoy entries of all sequences were concatenated to estimate error thresholds. The database processing used python scripts available at https://github.com/pwilmart/fasta_utilities.git, and Comet results processing used the PAW pipeline (46) from https://github.com/pwilmart/PAW_pipeline.git. Comet searches for all samples were performed with trypsin enzyme specificity with monoisotopic parent ion mass tolerance set to 1.25 Da and monoisotopic fragment ion mass tolerance of 1.0005 Da. A static modification of +57.02146 Da added to all cysteine residues and a variable modification of +15.9949 Da on methionine residues. Comet scores were used to compute linear

discriminant function scores (46, 47), and discriminant score histograms were created for 2+, 3+, and 4+ peptide charge states. Separate histograms were created for target matches and for decoy matches for all peptides of seven amino acids or longer. The score distributions of decoy matches were used to estimate peptide false discovery rates (FDR) and set score thresholds at 2% FDR for each peptide class (10,335 peptide spectrum matches passed thresholds). Protein inference used basic parsimony principles, and protein identifications required a minimum of 2 distinct peptide identifications per sample. Following filtering of common contaminants, this resulted in the identification of 540 proteins with one decoy protein match. The list of identified proteins is shown in Supplementary Table 1. The list of potential EWSR1-ATF1-interacting proteins was further filtered to consider only proteins having at least 3 unique peptides in the anti-Flag antibody group and 0 unique peptides in the IgG group, resulting in the identification of 6 proteins.

Western blot

The cells were treated with indicated drugs for different periods of time. Then, the cells were harvested by scraping and washed with cold PBS twice. The cell pellets were lysed in lysis buffer A supplemented with 8 M urea. The protein concentration of the samples was determined using BCA assay kit (Pierce), and equal amount of proteins was loaded onto 4 to 20% SDS-PAGE gel (Bio-Rad) for Western blot analysis using indicated antibodies.

ChIP assay

The ChIP assay was performed using EZ ChIP Chromatin Immunoprecipitation kit (Millipore) following the manufacturer's instructions. Briefly, DTC-1 cells were cross-linked with 1% formaldehyde. Then, the cells were lysed using provided SDS lysis buffer. The chromatin was sheared by sonication using FB120 probe sonicator (Fisher Scientific). The sheared chromatin was precleared using protein A/G bead slurry. The precleared chromatin was then immunoprecipitated using IgG, anti-CREB1, or anti-PRMT5 along with protein A/G bead slurry. After extensive washes with Low Salt Immune Complex Wash Buffer, High Salt Immune Complex Wash Buffer, LiCl Immune Complex Wash Buffer, and TE Buffer, the bound chromatin was eluted using 1% SDS in $NaHCO_3$. The eluted chromatin was then reverse cross-linked, and the resulting DNA was purified for qPCR analysis. The primers for *c-Fos* promoter were 5′- GGCCCACGAGACCTCTGAGACA-3′ (forward) and 5′- GCCTTGGCGCGTGTCCTAATCT-3′ (reverse).

MTT assay

The cells were plated in 96-well plates and were treated with indicated drugs at different concentrations for either 3 or 6 days. At the end of the treatment, the number of remaining viable cells was quantified using MTT reagent (Sigma, 0.5 mg/ml). The reduced purple formazan was dissolved in DMSO, and absorbance values at 570 nm were obtained from an i3 multimode plate reader (Molecular Devices). The percent of growth is defined as $100 \times (A_{treated} - A_{initial})/(A_{control} - A_{initial})$, where $A_{treated}$ represents absorbance in wells treated with a compound, $A_{initial}$ represents the absorbance at time 0, and $A_{control}$ denotes media-treated cells (38). The GI_{50} was derived from nonlinear regression analysis of the percent of growth–concentration curve in Prism 8.0.

SU-CCS-1 xenograft assay

The use of animals was approved by OHSU Institutional Animal Care and Use Committee (IACUC). SU-CCS-1 cells were prepared as a 1:1 mixture in Hank's Buffered Saline (HBS) and Matrigel (Corning). The 6-week-old athymic nude mice (Jax mice, female:male =1:1) were injected with 10 million cells subcutaneously to allow tumor intake. When the average tumor size reached ~100 mm^3, the mice were randomized to be treated with either vehicle or **JNJ-64619178** at 10 mg/kg once a day for 5 weeks (QDx5 weeks). The tumor volumes and body weights were measured every 2 or 3 days. The tumors were measured in two dimensions using a digital caliper, and the tumor volume was expressed in mm^3 using the formula $V = 0.5*a*b^2$, where a and b represent the long and short diameters of the tumor, respectively.

Statistical analysis

Student *t*-tests were used for calculating statistics, where a p value of less than 0.05 indicates significance. These tests were performed in Microsoft Excel (v 16.54).

Data availability

All data are within the article and its supporting information files.

Supporting information—This article contains supporting information.

Acknowledgments—We thank OHSU Massive Parallel DNA Sequencing Core for authenticating the cell lines and the OHSU Proteomic Shared Resource for protein identification. We graciously appreciated Dr. Nielsen for providing DTC-1 cell line and Dr. Keller for providing CCS292 cell line.

Author contributions—B. X. L. and X. X conceptualization; B. X. L. and L. L. D. data curation; B. X. L., L. L. D., L. E. D., and X. X. formal analysis; B. X. L. and X. X. funding acquisition; B. X. L. and X. X. project administration; B. X. L. and X. X. supervision; B. X. L. and X. X. validation; B. X. L. and X. X. writing- original draft preparation; B. X. L., L. L. D., L. E.D., and X. X writing – review & editing; L. L. D. software.

Funding and additional information—This work was made possible through financial supports provided from the National Institutes of Health R21CA220061 (X. X.), R01CA245964 (B. X. L.) and R01GM122820 (X. X.), Elsa U. Pardee Foundation, Oregon Health & Science University Technology Transfer Office, Oregon Health &

Science University School of Medicine. The proteomic analysis was partially supported by NIH grants P30EY010572 (L. L. D.) and P30CA069533 (L. L. D.). The content is solely the responsibility of the authors and does not necessarily represent the official views of the National Institutes of Health.

Conflict of interest—The authors declare that they have no conflicts of interest with the contents of this article.

Abbreviations—The abbreviations used are: ATF1, activating transcription factor 1; bZIP, basic leucine-zipper; CCS, clear cell sarcoma; CCSST, clear cell sarcoma of soft tissue; CBP, CREB-binding protein; ChIP, chromatin immunoprecipitation; CRE, cAMP-response element; CREB, CRE-binding protein; DMSO, dimethyl sulfoxide; EWSR1, EWS RNA binding protein 1; Fsk, forskolin; GO, gene ontology; IP, immunoprecipitation; MS, mass spectrometry; PKA, protein kinas A; PONDR, predictor of natural disordered regions; PRMT5, protein arginine methyltransferase 5; qPCR, quantitative polymerase chain reaction; RLuc, renilla luciferase.

References

1. Nacev, B. A., Jones, K. B., Intlekofer, A. M., Yu, J. S. E., Allis, C. D., Tap, W. D., *et al.* (2020) The epigenomics of sarcoma. *Nat. Rev. Cancer* **20**, 608–623
2. Enzinger, F. M. (1965) Clear-cell Sarcoma of tendons and aponeuroses. An analysis of 21 cases. *Cancer* **18**, 1163–1174
3. Mavrogenis, A., Bianchi, G., Stavropoulos, N., Papagelopoulos, P., and Ruggieri, P. (2013) Clinicopathological features, diagnosis and treatment of clear cell sarcoma/melanoma of soft parts. *Hippokratia* **17**, 298–302
4. Chung, E. B., and Enzinger, F. M. (1983) Malignant melanoma of soft parts. A reassessment of clear cell sarcoma. *Am. J. Surg. Pathol.* **7**, 405–413
5. Hocar, O., Le Cesne, A., Berissi, S., Terrier, P., Bonvalot, S., Vanel, D., *et al.* (2012) Clear cell sarcoma (malignant melanoma) of soft parts: A clinicopathologic study of 52 cases. *Dermatol. Res. Pract.* **2012**, 984096
6. Deenik, W., Mooi, W. J., Rutgers, E. J., Peterse, J. L., Hart, A. A., and Kroon, B. B. (1999) Clear cell sarcoma (malignant melanoma) of soft parts: a clinicopathologic study of 30 cases. *Cancer* **86**, 969–975
7. Kawai, A., Hosono, A., Nakayama, R., Matsumine, A., Matsumoto, S., Ueda, T., *et al.* (2007) Clear cell sarcoma of tendons and aponeuroses: A study of 75 patients. *Cancer* **109**, 109–116
8. Eckardt, J. J., Pritchard, D. J., and Soule, E. H. (1983) Clear cell sarcoma. A clinicopathologic study of 27 cases. *Cancer* **52**, 1482–1488
9. Cornillie, J., van Cann, T., Wozniak, A., Hompes, D., and Schoffski, P. (2016) Biology and management of clear cell sarcoma: State of the art and future perspectives. *Expert Rev. Anticancer Ther.* **16**, 839–845
10. Zucman, J., Delattre, O., Desmaze, C., Epstein, A. L., Stenman, G., Speleman, F., *et al.* (1993) EWS and ATF-1 gene fusion induced by T(12,22) translocation in malignant melanoma of soft parts. *Nat. Genet.* **4**, 341–345
11. Langezaal, S. M., Graadt van Roggen, J. F., Cleton-Jansen, A. M., Baelde, J. J., and Hogendoorn, P. C. (2001) Malignant melanoma is genetically distinct from clear cell sarcoma of tendons and aponeurosis (malignant melanoma of soft parts). *Br. J. Cancer* **84**, 535–538
12. Panagopoulos, I., Mertens, F., Debiec-Rychter, M., Isaksson, M., Limon, J., Kardas, I., *et al.* (2002) Molecular genetic characterization of the EWS/ATF1 fusion gene in clear cell sarcoma of tendons and aponeuroses. *Int. J. Cancer* **99**, 560–567
13. Ohno, T., Ouchida, M., Lee, L., Gatalica, Z., Rao, V. N., and Reddy, E. S. (1994) The EWS gene, involved in Ewing family of tumors, malignant melanoma of soft parts and desmoplastic small round cell tumors, codes for an RNA binding protein with novel regulatory domains. *Oncogene* **9**, 3087–3097
14. Shaywitz, A. J., and Greenberg, M. E. (1999) CREB: A stimulus-induced transcription factor activated by a diverse array of extracellular signals. *Annu. Rev. Biochem.* **68**, 821–861
15. Xiao, X., Li, B. X., Mitton, B., Ikeda, A., and Sakamoto, K. M. (2010) Targeting CREB for cancer therapy: friend or foe. *Curr. Cancer Drug Targets* **10**, 384–391
16. Gonzalez, G. A., and Montminy, M. R. (1989) Cyclic AMP stimulates somatostatin gene transcription by phosphorylation of CREB at serine 133. *Cell* **59**, 675–680
17. Lee, J., Nguyen, P. T., Shim, H. S., Hyeon, S. J., Im, H., Choi, M. H., *et al.* (2019) A multifunctional protein, regulates cellular function and aging via genetic and epigenetic pathways. *Biochim. Biophys. Acta Mol. Basis Dis.* **1865**, 1938–1945
18. Feng, L., and Lee, K. A. (2001) A repetitive element containing a critical tyrosine residue is required for transcriptional activation by the EWS/ATF1 oncogene. *Oncogene* **20**, 4161–4168
19. Yamada, K., Ohno, T., Aoki, H., Semi, K., Watanabe, A., Moritake, H., *et al.* (2013) EWS/ATF1 expression induces sarcomas from neural crest-derived cells in mice. *J. Clin. Invest.* **123**, 600–610
20. Straessler, K. M., Jones, K. B., Hu, H., Jin, H., van de Rijn, M., and Capecchi, M. R. (2013) Modeling clear cell sarcomagenesis in the mouse: Cell of origin differentiation state impacts tumor characteristics. *Cancer Cell* **23**, 215–227
21. Panza, E., Ozenberger, B. B., Straessler, K. M., Barrott, J. J., Li, L., Wang, Y., *et al.* (2021) The clear cell sarcoma functional genomic landscape. *J. Clin. Invest.* **131**, e146301
22. Wang, W. L., Mayordomo, E., Zhang, W., Hernandez, V. S., Tuvin, D., Garcia, L., *et al.* (2009) Detection and characterization of EWSR1/ATF1 and EWSR1/CREB1 chimeric transcripts in clear cell sarcoma (melanoma of soft parts). *Mod. Pathol.* **22**, 1201–1209
23. Hisaoka, M., Ishida, T., Kuo, T. T., Matsuyama, A., Imamura, T., Nishida, K., *et al.* (2008) Clear cell sarcoma of soft tissue: A clinicopathologic, immunohistochemical, and molecular analysis of 33 cases. *Am. J. Surg. Pathol.* **32**, 452–460
24. Davis, I. J., Kim, J. J., Ozsolak, F., Widlund, H. R., Rozenblatt-Rosen, O., Granter, S. R., *et al.* (2006) Oncogenic MITF dysregulation in clear cell sarcoma: Defining the MiT family of human cancers. *Cancer Cell* **9**, 473–484
25. Romero, P., Obradovic, Z., Li, X., Garner, E. C., Brown, C. J., and Dunker, A. K. (2001) Sequence complexity of disordered protein. *Proteins* **42**, 38–48
26. Jumper, J., Evans, R., Pritzel, A., Green, T., Figurnov, M., Ronneberger, O., *et al.* (2021) Highly accurate protein structure prediction with AlphaFold. *Nature* **596**, 583–589
27. Li, B. X., and Xiao, X. (2009) Discovery of a small-molecule inhibitor of the KIX-KID interaction. *Chembiochem* **10**, 2721–2724
28. Raudvere, U., Kolberg, L., Kuzmin, I., Arak, T., Adler, P., Peterson, H., *et al.* (2019) Profiler: A web server for functional enrichment analysis and conversions of gene lists (2019 update). *Nucleic Acids Res.* **47**, W191–W198
29. Wang, Y., Hu, W., and Yuan, Y. (2018) Protein arginine methyltransferase 5 (PRMT5) as an anticancer target and its inhibitor discovery. *J. Med. Chem.* **61**, 9429–9441
30. Chen, Y., Shao, X., Zhao, X., Ji, Y., Liu, X., Li, P., *et al.* (2021) Targeting protein arginine methyltransferase 5 in cancers: roles, inhibitors and mechanisms. *Biomed. Pharmacother.* **144**, 112252
31. Tsai, W. W., Niessen, S., Goebel, N., Yates, J. R., 3rd, Guccione, E., and Montminy, M. (2013) PRMT5 modulates the metabolic response to fasting signals. *Proc. Natl. Acad. Sci. U. S. A.* **110**, 8870–8875
32. Hwang, J. W., Cho, Y., Bae, G. U., Kim, S. N., and Kim, Y. K. (2021) Protein arginine methyltransferases: Promising targets for cancer therapy. *Exp. Mol. Med.* **53**, 788–808
33. Araya, N., Hirota, K., Shimamoto, Y., Miyagishi, M., Yoshida, E., Ishida, J., *et al.* (2003) Cooperative interaction of EWS with CREB-binding protein selectively activates hepatocyte nuclear factor 4-mediated transcription. *J. Biol. Chem.* **278**, 5427–5432
34. Rossow, K. L., and Janknecht, R. (2001) The Ewing's sarcoma gene product functions as a transcriptional activator. *Cancer Res.* **61**, 2690–2695
35. Chan-Penebre, E., Kuplast, K. G., Majer, C. R., Boriack-Sjodin, P. A., Wigle, T. J., Johnston, L. D., *et al.* (2015) A selective inhibitor of PRMT5

with *in vivo* and *in vitro* potency in MCL models. *Nat. Chem. Biol.* **11**, 432–437

36. Duncan, K. W., Rioux, N., Boriack-Sjodin, P. A., Munchhof, M. J., Reiter, L. A., Majer, C. R., *et al.* (2016) Structure and property guided design in the identification of PRMT5 tool compound EPZ015666. *ACS Med. Chem. Lett.* **7**, 162–166
37. Brehmer, D., Beke, L., Wu, T., Millar, H. J., Moy, C., Sun, W., *et al.* (2021) Discovery and pharmacological characterization of JNJ-64619178, a novel small molecule inhibitor of PRMT5 with potent anti-tumor activity. *Mol. Cancer Ther.* **20**, 2317–2328
38. Xie, F., Li, B. X., Kassenbrock, A., Xue, C., Wang, X., Qian, D. Z., *et al.* (2015) Identification of a potent inhibitor of CREB-mediated gene transcription with efficacious *in Vivo* anticancer activity. *J. Med. Chem.* **58**, 5075–5087
39. Jensen-Pergakes, K., Tatlock, J., Maegley, K. A., McAlpine, I. J., McTigue, M. A., Xie, T., *et al.* (2022) SAM competitive PRMT5 inhibitor PF-06939999 demonstrates antitumor activity in splicing dysregulated NSCLC with decreased liability of drug resistance. *Mol. Cancer Ther.* **21**, 3–15
40. Alinari, L., Mahasenan, K. V., Yan, F., Karkhanis, V., Chung, J. H., Smith, E. M., *et al.* (2015) Selective inhibition of protein arginine methyltransferase 5 blocks initiation and maintenance of B-cell transformation. *Blood* **125**, 2530–2543
41. McKinney, D. C., McMillan, B. J., Ranaghan, M. J., Moroco, J. A., Brousseau, M., Mullin-Bernstein, Z., *et al.* (2021) Discovery of a first-in-class inhibitor of the PRMT5-substrate adaptor interaction. *J. Med. Chem.* **64**, 11148–11168
42. Davis, I. J., McFadden, A. W., Zhang, Y., Coxon, A., Burgess, T. L., Wagner, A. J., *et al.* (2010) Identification of the receptor tyrosine kinase c-Met and its ligand, hepatocyte growth factor, as therapeutic targets in clear cell sarcoma. *Cancer Res.* **70**, 639–645
43. Schöffski, P., Wozniak, A., Stacchiotti, S., Rutkowski, P., Blay, J. Y., Lindner, L. H., *et al.* (2017) Activity and safety of crizotinib in patients with advanced clear-cell sarcoma with MET alterations: european organization for research and treatment of cancer phase II trial 90101 'CREATE. *Ann. Oncol.* **28**, 3000–3008
44. Li, B. X., Chen, J., Chao, B., Zheng, Y., and Xiao, X. (2018) A lamin-binding ligand inhibits homologous recombination repair of DNA double-strand breaks. *ACS Cent. Sci.* **4**, 1201–1210
45. Eng, J. K., Jahan, T. A., and Hoopmann, M. R. (2013) Comet: An open-source MS/MS sequence database search tool. *Proteomics* **13**, 22–24
46. Wilmarth, P. A., Riviere, M. A., and David, L. L. (2009) Techniques for accurate protein identification in shotgun proteomic studies of human, mouse, bovine, and chicken lenses. *J. Ocul. Biol. Dis. Infor.* **2**, 223–234
47. Keller, A., Nesvizhskii, A. I., Kolker, E., and Aebersold, R. (2002) Empirical statistical model to estimate the accuracy of peptide identifications made by MS/MS and database search. *Anal. Chem.* **74**, 5383–5392